Identification of Arsenic Spatial Distribution by Hydrogeochemical Processes Represented by Different Ion Ratios in the Hohhot Basin, China

Yu Ren
Institute of Hydrogeology and Environmental Geology
Wengeng Cao (281084632@qq.com)
Institute of Hydrogeology and Environmental Geology https://orcid.org/0000-0001-5693-5292
Zeyan Li
Institute of Hydrogeology and Environmental Geology
Deng Pan
Henan Institute of Geological Environmental Monitoring
Shuai Wang
Henan Institute of Geological Environmental Monitoring

Research Article

Keywords: Hohhot Basin, high arsenic groundwater, ion ratio, cumulative frequency curve

Posted Date: June 6th, 2022

DOI: https://doi.org/10.21203/rs.3.rs-1527775/v1

Abstract

The Hohhot Basin, a typical inland basin of the Yellow River Basin in China, generally has high concentrations of arsenic (As) in its shallow groundwater, while the factors dominating the distribution of high arsenic levels remain to be further identified. An analysis of the ratio of hydrogeochemical compositions can help to reveal the spatial characteristics of the shallow groundwater environmental conditions and the distribution of high arsenic water (As > 10μg/L). In this study, a total of 170 samples of shallow groundwater in the Hohhot Basin were collected and water samples with As > 10μg/L accounted for 29.4% of the total. Based on the slope changes of the cumulative frequency curves of $(HCO_3^- + CO_3^{2-})/SO_4^{2-}$, $Ca^{2+}/(HCO_3^- + CO_3^{2-})$, Ca^{2+}/Mg^{2+} and Na^+/Ca^{2+}, the groundwater in the study area can be categorized into six different zones according to the environmental characteristics including redox condition, surface water recharge intensity and cation exchange level. The result shows that the groundwater in the front of the piedmont alluvial plain and platform is in a weak reducing condition with high lateral recharge intensity, fast runoff, and weak cation exchange. In the Dahei River alluvial plain, which serves as the groundwater discharge zone, the groundwater runoff is sluggish with poor lateral recharge, sufficient exchange between cations in the groundwater and the aquifer matrix, and enhanced reducibility. The degree of oxidation increased in the groundwater near the Hasuhai Lake and the drainage canal, which adverse to the arsenic enrichment. High arsenic groundwater is mainly distributed in aquifers of $(HCO_3^- + CO_3^{2-})/SO_4^{2} > 10$, $Na^+/Ca^{2+} > 13$, and $Ca^{2+}/(HCO_3^- + CO_3^{2-}) < 0.1$, which represent the strong reducing condition, low surface water recharge intensity and strong cation exchange condition. Reductive dissolution of iron oxide, strong evaporation and concentration process, and competition from phosphate in aquifers jointly lead to the release of arsenic into groundwater.

1. Introduction

Arsenic, a common nonmetallic element in groundwater, can cause neurological and skin diseases if ingested at high concentrations. Long-term exposure can lead to increased cancer risks to the liver, bladder and other organs (Danrui et al. 2021, Silvera and Rohan 2007, Yu and Habibu 2004). Both the World Health Organization (WHO) and China set the standard that the maximum concentration of arsenic in drinking water is 10μg/L. High arsenic groundwater is widely present in more than 70 countries such as Bangladesh, India, the United States and China, and affects approximately 100–200 million global population (Kumar and T. 2002, Scott et al. 2010, Yanxin et al. 2019).

The formation of high arsenic groundwater is mainly caused by geological origin and human activities (Kirk 2002). High arsenic groundwater from geological origin primarily occurs in rivers, lake basins or river deltas and can be enriched by means of leaching-enrichment, burial-dissolution, compaction-release and evaporation-concentration (Xiaodong et al. 2020, Wang Yanxin et al. 2020). The distribution of high arsenic groundwater in Bangladesh and China indicates that it mainly occurs in the anaerobic reductive environment of Holocene strata (Guo Huaming et al. 2011, Yan et al. 2004). The high arsenic groundwater is generally in a weak alkaline environment with high Fe and Mn concentrations. In the

reducing environment, arsenic could be released into the groundwater through the reduction dissolution of iron and manganese oxides (Guo Huaming et al. 2008, Xiaodong et al. 2020). However, the chemical characteristics of groundwater differ between inland basins and delta areas. For example, HCO_3^-, Na^+ and TDS are in high levels in Datong Basin and Hetao plain, while the distribution of cations is dispersive in high arsenic river deltas (Guo Huaming et al. 2014, Xianjun et al. 2009, Xiaodong et al. 2020).

China is one of the countries severely affected by high arsenic groundwater, especially in the Yellow River basin (Han et al. 2021), including Yinchuan Basin (Qi et al. 2014), Hetao Basin (Guo Huaming et al. 2014) and Xinxiang area which locates in the lower reaches of the Yellow River (Ren et al. 2021). The Hohhot Basin is located in the upper and middle reaches of the Yellow River basin and its shallow groundwater is widely used for agriculture but with a high arsenic level of 300μg/L (Guo Huaming et al. 2014, L. et al. 2003). The high concentrations of arsenic in the groundwater of the Hohhot Basin are the consequence of the area's geomorphic characteristics and mainly exist in the lowest river flat.

Considering the great spatial variability of the arsenic occurrence, scholars have adopted different approaches to identify the characteristics of arsenic spatial distribution. In the Hetao Basin, indicators including the soil-sand ratio and the number of clay layers are positively correlated with the concentration of arsenic, making it convenient to identify high arsenic areas (Cao Wengeng et al. 2017). The concentrations of stable isotopes of carbon, hydrogen and oxygen are likewise positively correlated with the arsenic content in groundwater (Yinzhu et al. 2018), Fe and S isotopes also gather in high arsenic groundwater (Guo Huaming et al. 2013, Yanxin et al. 2014). The ratio of different ions can indicate the hydrogeochemical formation of the groundwater (Jia Yongfeng et al. 2017) in that $Ca^{2+}/(HCO_3^-+CO_3^{2-})$ shows the intensity of lateral recharge while SO_4^{2-}/Cl^- and HCO_3^-/SO_4^{2-} reflects the degree of groundwater reducibility in arid and semi-arid areas (Cao Wengeng et al. 2017, Jia Yongfeng et al. 2014). Because of the great stability of major hydrogeochemical compositions of the groundwater, it is relatively accurate to conclude groundwater environmental characteristics from analysis of specific ion ratios. The cumulative frequency distribution curves of various ion ratios demonstrate the accumulative process of different groundwater ratios from 0 to 100%. The obvious changes in the slope of the cumulative frequency curve mean that the distribution range of the ratio has changed greatly, revealing a significant change in the groundwater environment (Armstrong 2004, Clemens et al. 2005). Therefore, changes in the slope of cumulative frequency curves can help divide the study area for research purposes.

In this paper, the shallow groundwater in the Hohhot Basin is divided into several zones based on the spatial distribution characteristics and the changes in cumulative frequency curves representing four types of ion ratios, which serves to (1) analyze the different types of hydrogeochemical processes in the shallow groundwater of the study area; (2) provide a new method for identifying the spatial distribution of high arsenic content by cumulative frequency curves of ion ratios; and (3) establish a model of hydrogeochemical reactions in zones divided according to different ion ratios.

2. Overview Of The Study Area

2.1 Geographic feature

The Hohhot Basin is located in Inner Mongolia of China, where the terrain slopes from northeast to southwest in general and from north to south in the west (Fig. 1). The plain is narrow in the west and wide in the east, and the Yellow River flows east along the southern edge of the plain. The eastern plain is covered by alluvial deposits of the Dahei River and thick lake deposits gather in the lower part. On the easter part of the plain lies the Manhan Mountain, southern part the Horinger platform, and northern part the Daqing Mountain. The flat terrain slightly inclines to the west and the surface lithology is mainly Holocene (Q4) sandy loam in the Dahei River alluvial plain.

2.2 Hydrology and meteorology

The Hohhot Basin is in an arid and semi-arid climate with obvious seasonal variations, long winter time and short summer time. This climate is characterized by low precipitation, high evaporation and high diurnal temperature. The Dahei River in the study area, a tributary of the Yellow River, consists of three parts: the mainstream of Dahei River in the east, the tributaries in the west, as well as Hasuhai Lake and drainage canal.

2.3 Hydrogeological condition

The monolayer aquifer is distributed in front of Daqing Mountain, Manhan Mountain and the northern edge of the Horinger platform. It contains coarse grains and has good hydraulic connections yet is devoid of stable and continuous waterproof layers. The double-layer aquifer is distributed in front of the piedmont inclined plain and alluvial plain of the basin center.

In the monolayer aquifer, the shallow groundwater is mainly recharged by the lateral runoff from the groundwater in the mountainous area and discharged by flowing to the double layer aquifer and artificial exploitation. The shallow groundwater in the double-layer aquifer is primarily recharged by lateral runoff from the monolayer aquifer, and secondarily recharged by other sources including precipitation, canal system infiltration, irrigation infiltration, and leaking recharge from confined groundwater.

The shallow groundwater in the piedmont plain mainly flows from northeast to southwest, east to west, or southeast to northwest. In the piedmont alluvial plain, the aquifer particles are coarse, resulting in a large permeability coefficient and hydraulic gradient. Meanwhile, the runoff rate is fast and the shallow water is mainly discharged by runoff. When entering the Dahei River alluvial plain, the groundwater mainly flows from northeast to southwest. Due to the gentle topography and fine particles of the aquifer in the alluvial plain, the hydraulic gradient of groundwater decreases and the groundwater runoff rate becomes very slow.

3. Materials And Methods

3.1 Field sampling

In this study, a total of 170 groundwater samples were collected in 2016. All samples were from shallow water, i.e. well depths were less than 100m. The water sample containers were cleaned with well water 3 times and then filled with water samples, ensuring that no gaps were left at the top after the protective agent is added. Then immediately the water sample containers were tightly capped, sealed with tapes and labeled. All water samples would be analyzed and tested in the laboratory within 7 days.

3.2 Tests and analytical method

(1) Site test

The water temperature, pH conductivity (EC), and total dissolved solids (TDS) were tested by sensION + MM150(MM156) portable multi-parameter water quality analyzer produced by HACH Company, and the turbidity was tested by WGZ-200B portable turbidimeter (meter) produced by Shanghai Xingrui Company.

(2) Laboratory test

K^+, Na^+, Ca^{2+}, Mg^{2+}, Fe, Mn, and other cations were measured by inductively coupled plasma atomic emission spectroscopy (ICP-AES) and inductively coupled plasma mass spectroscopy (ICP-MS) in the laboratory of the Institute of Hydrogeology and Environmental Geology (IHEG), Chinese Academy of Geological Sciences (CAGS). The arsenic content in groundwater was measured by inductively coupled plasma mass spectroscopy (ICP-MS) (7500C, Agilent). The error range of cation and anion concentration for all samples was less than 5%, ensuring the accuracy of all data.

(3) Division method of the cumulative frequency curve

The cumulative frequency curve can show the accumulative distribution in the ratios of different hydrogeochemical compositions. As the ratio grows and the number of samples increases, the cumulative frequency increases from 0 to 100%. All data would form different straight lines on the curve and the inflection point (threshold) at which the slope changes would exhibit a significant increase in the cumulative number of ratios. The significant change in the slope of the straight line indicates a change in the groundwater environment and chemical processes (María et al. 2007). Therefore, in this study, the cumulative frequency curve of ion ratios was plotted, and the line was divided into several ratio ranges according to different slopes, which were displayed on the map. Finally, according to the ranges and spatial distributions of ratios, the hydrogeochemical differences in groundwater were determined, revealing the chemical processes in groundwater of different areas.

4. Results

4.1 Hydrogeochemical distribution of groundwater

The concentration ranges of ions and TDS in 170 samples differed from two to three orders of magnitude (Table 1), indicating strong spatial variability of shallow groundwater in the study area. The pH of shallow groundwater in the Hohhot Basin was slightly alkaline, ranging from 7.25 to 9.05. The types of

anion and cation with the highest concentration were HCO_3^- and Na^+, with a median value of 378 and 98.3mg/L respectively. TDS ranged from 262 to 6.11×10^3mg/L, with a median value of 579mg/L and saline water (TDS > 1g/L) accounted for 28.8% of the total.

The Ca^{2+} concentration was 5.70–260mg/L, and the groundwater with a high Ca^{2+} content was mainly distributed in the piedmont plain of Daqing Mountain and Manhan Mountain with strong runoff. The Na^+ concentration ranged from 9.93 to 2.10×10^3mg/L, and the groundwater with high Na^+ concentration was distributed in the alluvial plain of Dahei River, which is the main discharge region in the study area. Meanwhile, Na^+ and TDS showed a linear positive correlation (R^2 = 0.898), indicating that high TDS in groundwater was affected by the increase of Na^+ concentration (Figure S1). The piper diagram showed that water chemical types were correlated with arsenic concentration.

In high arsenic groundwater (As > 10μg/L), the concentrations of Na^+ and HCO_3^- increased to 26.3–1.62×10^3 and 277–2.12×10^3mg/L, with a median value of 114 and 430mg/L respectively. However, the concentration of Ca^{2+} decreased to 5.70–156mg/L, with a median value of 42.5mg/L, indicating that the high arsenic water was enriched towards salinization, especially in groundwater with As > 50μg/L where the main hydrogeochemical type is Na-HCO_3 (Fig. 2).

4.2 Spatial distribution of arsenic

The overall arsenic concentrations in the groundwater of the Hohhot Basin ranged from 0.05 to 357.5μg/L, with an average value of 26.9μg/L and a median value of 3.15μg/L (Table 1). High arsenic groundwater (As > 10μg/L) accounted for 29.4% of the total. To further identify the distribution characteristics of arsenic in shallow groundwater of different geomorphic units, the 170 water samples were divided into three groups according to different arsenic concentrations, namely 0–10, 10–50, and > 50μg/L. An analysis of the concentration and spatial distribution of arsenic in the study area revealed that the distribution of arsenic was affected by the sedimentary environment. Most of the arsenic groundwater was distributed in the alluvial plain of Dahei river, and a small part of it was distributed along the Yellow River and near Hasuhai Lake (Fig. 3). Specifically, water with arsenic levels above 50μg/L was concentrated in the alluvial plain of Dahei River, while the arsenic levels in other areas were generally below 10μg/L. The low arsenic groundwater was mainly distributed in wells with depths of 0–70m but the high arsenic groundwater is concentrated in wells of 0–40m depth, indicating that the shallower aquifers are more favorable for arsenic enrichment in groundwater.

4.3 Cumulative frequency curves and distribution characteristics of ion ratios

(1) $(HCO_3^- + CO_3^{2-})/SO_4^{2-}$

In the reducing environment of arid and semi-arid areas, sulfates are converted into S^{2-} under the reactions of microorganisms, and the concentration of HCO_3^- increases through the oxidative

transformation of organic compounds (Huaming et al. 2008, L. et al. 2003). In this climate, (HCO_3^- +CO_3^{2-})/SO_4^{2-} increases with the enhancement of groundwater reducibility, so it can be used as an indicator of the groundwater redox status. Most groundwater samples in Group 1 were distributed around Hasuhai Lake and the drainage canal and a small part were distributed in the southeast of the study area. Samples in Group 2 and 3 were mainly distributed in the piedmont areas of Daqing Mountain in the north, Horinger platform in the south, and Manhan Mountain in the east. Samples in Group 4 were mainly distributed in the groundwater discharge zone of the Daqing Mountain piedmont alluvial plain front and the Dahei River alluvial plain (Fig. 4).

(2) $Ca^{2+}/(HCO_3^- + CO_3^{2-})$

The Ca^{2+} content in groundwater can indicate the degree of recharge by surface water (Wengeng et al. 2017). The Ca^{2+} content increases with the enhancement of surface water recharge intensity. According to the slope change of the $Ca^{2+}/(HCO_3^-+CO_3^{2-})$ cumulative frequency curve, the study area can be divided into four groups. Group 1 samples were distributed in the west of the Dahei River plain, while Group 2 samples were located in the east of the Dahei River, the Horinger platform front and the front of the Daqing Mountain piedmont alluvial plain. Group 3 samples were mainly distributed in the Daqing Mountain piedmont alluvial plain and east of the Horinger platform. Group 4 samples were mainly distributed in the Manhan Mountain piedmont alluvial plain. Along the flow direction of the groundwater from the piedmont plain to the river plain, the $Ca^{2+}/(HCO_3^-+CO_3^{2-})$ index gradually decreases, indicating that the groundwater is less affected by lateral recharge.

(3) Ca^{2+}/Mg^{2+}

The Ca^{2+}/Mg^{2+} ratio also reflects the intensity of groundwater lateral recharge, in that the increase of the former can manifest the enhancement of the latter. Based on the slope change of the Ca^{2+}/Mg^{2+} cumulative frequency curve (Fig. 6), the study area was divided into four groups: 1(0-0.4), 2(0.4–1.4), 3(1.4–2.2) and 4(> 2.2). Group 1 water was mainly distributed in the Dahei River alluvial plain and near the Hasuhai Lake. Group 2 groundwater was mainly located in the Daqing Mountain alluvial plain, the eastern Dahei River alluvial plain and near the Horinger platform. Groups 3 and 4 groundwater were mainly distributed in the piedmont plain of the Manhan Mountain.

(4) Na^+/Ca^{2+}

Cation exchange between groundwater and minerals of aquifers occurs when local runoff conditions are poor. The Na^+/Ca^{2+} ratio can indicate the cation exchange degree in groundwater (Chengcheng et al. 2020). With the enhancement of cation exchange, both the Na^+ content and the ratio of Na^+/Ca^{2+} gradually increase. According to the slope change of the Na^+/Ca^{2+} cumulative probability curve, the study area can be divided into four groups: 1(0-1.1), 2(1.1–2.4), 3(2.4–13), and 4(> 13) (Fig. 7). Group 1 groundwater was mainly distributed in the vicinity of the Hasuhai Lake, the drainage canal and the

alluvial plain of the Manhan Mountain. Group 2 groundwater was mainly located near the Daqing Mountain alluvial plain and the southern Horinger platform. Group 3 groundwater was widely distributed in the margin of the Dahei River alluvial plain, while Group 4 groundwater was concentrated in the discharge center of the Dahei River alluvial plain.

5. Discussion

5.1 Recognition of arsenic spatial distribution characteristics by different ion ratios

Since the occurrence of arsenic is significantly affected by hydrogeochemical processes in the groundwater environment, the distribution characteristics of different ion ratios can not only help to identify hydrogeochemical processes in groundwater, but also effectively facilitate identifying the distribution mechanism of arsenic in the study area. In the light of the concentration characteristics and spatial distribution of different ion ratios in the foregoing sections, the groundwater in the study area was divided into six zones according to the final boundary that was set according to boundaries of overlapping areas of the four ion ratios (Fig. 8).

The Manhan Mountain piedmont alluvial plain zone (Zone I) was characterized by $Na^+/Ca^{2+}<1.1$, $Ca^{2+}/(HCO_3^-+CO_3^{2-}) > 0.7$, and $Ca^{2+}/Mg^{2+}>1.4$, indicating that groundwater was mainly distributed in this area (Fig. 8A). The median value of Ca^{2+} concentration in this zone was 69.7mg/L, which was the highest among the five zones (Table S1). The high Ca^{2+} concentration reflected that groundwater was strongly influenced by surface water. This was mainly caused by strong piedmont lateral recharge considering the geomorphological characteristics of this area. The low Na^+ content indicated a weak cation exchange and a good groundwater runoff condition in this area. The mean value of arsenic concentration in this region is 1.08μg/L and the arsenic concentration of all samples is less than 10μg/L, which is the lowest among the six regions.

The Horinger platform zone (Zone II) was characterized by groundwater with ion ratio $0.4 < Ca^{2+}/Mg^{2+} <1.4$, $2<(HCO_3^-+CO_3^{2-})/SO_4^{2-}<5$, and $0.1 < Ca^{2+}/(HCO_3^-+CO_3^{2-}) < 0.5$ in the northern front of Horinger platform (Fig. 8B).The median values of Na^+, $Ca^{2+}$and Mg^{2+} concentration in this zone were 165, 40.7 and 45.2mg/L respectively (Table S1). The values of Ca^{2+}/Mg^{2+} and $Ca^{2+}/(HCO_3^-+CO_3^{2-})$ indicated that the Ca^{2+} content in this area was relatively lower than that in the vicinity of the Hasuhai Lake and the Manhan Mountain, but higher than that in the Dahei River alluvial plain, representing that the groundwater was weakly recharged from the platform region. The value of $(HCO_3^-+CO_3^{2-})/SO_4^{2-}$ indicated that the redox condition of groundwater is in a weak reducing state. The average arsenic concentration of groundwater in this area was 3.33μg/L, and only one water sample with As > 10μg/L was distributed in Zone II.

The Daqing Mountain piedmont alluvial plain zone (Zone III) is located in the alluvial plain in front of Daqing Mountain (Fig. 8B) with ion ratios of $2<(HCO_3^- + CO_3^{2-})/SO_4^{2-}<5$ and $0.5 < Ca^{2+}/(HCO_3^- + CO_3^{2-}) < 0.7$. The ion ratio indicated that the groundwater in this place was under weak reducing and runoff conditions. The groundwater was affected by the lateral recharge in front of Daqing Mountain, which is stronger than the lateral recharge in the Horinger platform. The mean value of arsenic concentration in this area was 17.8μg/L, and the groundwater had a low arsenic level near the mountain front but a high arsenic level near the Dahei River alluvial plain.

The transition zone (Zone IV) was represented by ion ratios of $0.4 < Ca^{2+}/Mg^{2+}<1.4$, $5<(HCO_3^- + CO_3^{2-})/SO_4^{2-}<10$, and $0.1 < Ca^{2+}/(HCO_3^- + CO_3^{2-}) < 0.5$ in the transition zone between the piedmont alluvial plain and the Dahei River alluvial plain(Fig. 8C). The ion ratios demonstrated that the groundwater in Zone IV was affected by a weak lateral recharge and medium reducing environment that was stronger than Zone II and Zone III. The median value of arsenic concentration was 17.9μg/L and 47.4% of water samples had arsenic levels higher than 10μg/L.

The Dahei River alluvial plain zone (Zone V) was mainly situated in the groundwater discharge area of Dahei River alluvial plain (Dongguang et al. 2013) in view of the distribution range of $(HCO_3^- + CO_3^{2-})/SO_4^{2} > 10$ and $Na^+/Ca^{2+}>13$, $Ca^{2+}/(HCO_3^- + CO_3^{2-}) < 0.1$ (Fig. 8D). The ratio of groundwater with $(HCO_3^- + CO_3^{2-})/SO_4^{2-}>10$ was the highest in the study area, indicating the strongest reducibility of groundwater in this area. The median values of Ca^{2+} and Na^+ concentration were 28.2 and 215mg/L, which respectively were the minimum and maximum values in all zones (Table S1). The ratios of $Ca^{2+}/(HCO_3^- + CO_3^{2-})$, Na^+/Ca^{2+} and ion content jointly indicated that the surface water recharge effect of Zone IV is the weakest in the whole study area, and neither the Hasuhai Lake nor the piedmont groundwater can recharge to the groundwater of this area. At the same time, the cation exchange between Ca^{2+} in the aquifer and Na^+ in the groundwater is sufficient. The average arsenic concentration in the groundwater of Zone IV reached 91.6μg/L, which is significantly higher than that in other zones.

The drainage canal zone (Zone VI) had groundwater with $Na^+/Ca^{2+}<1.1$ and $(HCO_3^- + CO_3^{2-})/SO_4^{2-}<2$ that was mainly distributed in the east of the Hasuhai Lake and the drainage canal (Fig. 8C). The mean value of arsenic concentration in the groundwater of this area is 10.0μg/L. The ratio of $(HCO_3^- + CO_3^{2-})/SO_4^{2-}$ in Zone VI is the smallest in the study area, indicating the strongest oxidation degree of groundwater. Studies have shown that the groundwater was affected by the quality of its nearby lakes and canals (Huaming et al. 2011, Søren et al. 2012). Groundwater will be mixed with surface water of higher oxygen content, resulting in increased oxidation of the groundwater. Besides, the Na^+/Ca^{2+} ratio of Zone VI is the smallest in the study area, indicating a weak cation exchange between Ca^{2+} and Na^+ in the aquifer and a good runoff condition. It is worth noting that although the Na^+/Ca^{2+} value in Zone VI is the smallest in the whole study area, the median and mean value of Na^+ concentration were 203 and 298mg/L respectively, which were only lower than that in Zone V among the six zones. Meanwhile, its TDS, Mg^{2+} and SO_4^{2-}

concentrations were the highest in the study area, and the median and average values of Ca^{2+} were only lower than that of Zone I (Table S1).

It can be concluded that the distribution of arsenic and ion ratio in groundwater had significant consistent characteristics. The median value of arsenic concentration in the six zones were 0.785, 2.76, 2.87, 4.30, 54.3 and 2.48μg/L respectively (Fig. 9a). It can be found that the total arsenic content of Zone V was significantly higher than that of other zones, while the total arsenic content in Zone I was the lowest. The arsenic concentration of Zone II, III, IV and VI were roughly similar, between Zone V and IV. The result of ion ratios revealed that Zone V had the weakest lateral recharge but the strongest reduction and cation exchange. In contrast, Zone I had the strongest piedmont lateral recharge effect and the best runoff condition among the six zones.

Therefore, the occurrence characteristics of arsenic can be identified by the value distribution of the four kinds of ion ratios (Table 2). High arsenic groundwater was distributed in the groundwater discharge zone of the Dahei River alluvial plain. This zone was in a strong reducing environment with high $(HCO_3^- + CO_3^{2-})/SO_4^{2-}$, low $Ca^{2+}/(HCO_3^- + CO_3^{2-})$ and low Ca^{2+}/Mg^{2+}, indicating that it was not affected by surface water recharge. Meanwhile, under the poor runoff conditions of the groundwater, the increase of Na^+/Ca^{2+} ratio represented a strong cation exchange. The low-arsenic area, affected by recharge from piedmont and the Hasuhai Lake, had good groundwater runoff, which was not conducive to arsenic release.

5.2 Hydrogeochemical processes in different zones

In Zone V, which had the highest arsenic concentration, the depth to the water table is shallow, ranging between 1.33 and 7.83m (Fig. 9c), with a median value of 2.68m. The median TDS in this zone reached 901.3mg/L. The median depth to the water table and TDS in Zone VI were 2.7m and 1416mg/L respectively (Table S1). Zone V and VI showed the shallowest water level in all zones (Fig. 9a, b). There was a significant negative correlation between arsenic content and water level (Fig. 10A), in other words, shallower groundwater had higher arsenic levels. Therefore, it suggested that strong evaporation and concentration occurred in Zone V and VI (L. and G. 2002, Liu et al. 2017), and arsenic was further enriched under evaporation concentration (Dongguang et al. 2013). This also explained that although cation exchange was strong in Zone IV, the Na^+ content was still significantly higher than that in the piedmont plain and platform. On the contrary, the median value of the groundwater table and TDS reached 14.09m and 477.1mg/L respectively in Zone I, meaning that the groundwater was not affected by evaporation and TDS also showed desalination characteristics (Fig. 9C and Table S1).

Arsenic and iron concentration in groundwater were positively correlated (Fig. 10b), indicating that the release of arsenic was related to the increase of iron content. It showed that the groundwater in Zone V had the strongest reducing condition and also the highest concentration of iron in the basin, with a median concentration of 0.48mg/L (Table S1). Under the reducing condition, iron oxide gained electrons and dissolved into ferrous ions into groundwater through reductive dissolution. Arsenic adsorbed on iron

oxide was released into the groundwater (L. et al. 2003, Ting et al. 2012). The low arsenic areas were affected by the recharge of oxygen-bearing surface water and had a low iron content.

Ammonia-nitrogen and nitrate-nitrogen concentrations were greatly affected by redox conditions hence they could be considered as sensitive indicators of redox. The transformation of nitrogen in the groundwater was also significantly different. Arsenic concentration was negatively correlated with nitrate concentration but positively correlated with ammonium concentration (Fig. 10c, d). In other words, nitrate concentration was significantly lower in high arsenic groundwater while ammonium concentration was higher in low arsenic groundwater (Qi et al. 2014, Shuangbao et al. 2013) (Fig. 9a, e and f). The NO_3^- concentration was found to be the highest in Zone I and IV, where oxidation was the strongest, with the median concentration reaching 28.8 and 42.2mg/L respectively. Meanwhile, the median ammonium concentration in these two zones (0.02mg/L and 0.04mg/L) was significantly lower than that of other zones. The groundwater in Zone VI and I were affected by oxygenated water recharge from the Hasuhai Lake and the drainage canal as well as lateral recharge from the Manhan Mountain, and therefore the oxidation of Zone I and IV were significantly higher than that in other zones (Huaming et al. 2010). Ammonia-nitrogen in oxidized groundwater would be converted to nitrate nitrogen by nitrification (Marco et al. 2017). Low nitrate-nitrogen (median 3.08mg/L) and high ammonium nitrogen (median 0.16mg/L) were found in Zone V. Compared with the Manhan Mountain piedmont plain, the concentration of ammonia nitrogen in Zone V significantly increased while the concentration of total inorganic nitrogen decreased (Figure S2). Groundwater was in an anaerobic state under the strong reducing condition of Zone V. In the presence of organic compounds, nitrate-nitrogen not only released N_2 through denitrification but also transformed into ammonium nitrogen through dissimilatory nitrate reduction to ammonium (DNRA) reaction (T. et al. 2011, Zhipeng et al. 2021).

Meanwhile, the median concentration of HPO_4^{2-} in Zone V reached 1.2mg/L, which was significantly higher than that in other zones (Fig. 9d and Table S1). The release of phosphorus (P) under anoxic conditions was mainly controlled by the reductive dissolution of iron oxide (Yao et al. 2022). The high phosphate concentration promoted the release of arsenic in groundwater by competing for adsorption sites (L. and G. 2002). There was no evident correlation between F and As in the study area (Fig. 10e). Highly fluoridated groundwater was mainly found in Zone II and V, where the Na^+ level was high. Because Ca^{2+} and F^- in groundwater were able to form fluorite precipitation, high Ca^{2+} was not conducive to the enrichment of fluoride. Arsenic enrichment was enhanced by weak evaporation and concentration due to the shallow water level, but the weak runoff and oxidation environment inhibited the release of arsenic into groundwater in Zone II and III. The position and ion ratios of Zone IV manifested that the environment of the transition zone slightly promoted the release of arsenic. Thus, as the aquifer environment altered along the direction of groundwater runoff, the arsenic release mechanism and the hydrogeochemical action model changed accordingly (Fig. 11).

6. Conclusion

In this study, the slope change thresholds of the cumulative frequency curves of $(HCO_3^- + CO_3^{2-})/SO_4^{2-}$, $Ca^{2+}/(HCO_3^- + CO_3^{2-})$, Ca^{2+}/Mg^{2+} and Na^+/Ca^{2+} were confirmed to identify the spatial ranges of different types of physical and chemical processes in the shallow groundwater of the Hohhot Basin. The groundwater in the Basin was divided into six zones accordingly. The arsenic concentration in the groundwater of the Manhan Mountain piedmont alluvial plain zone was 0.785μg/L (median value, the same below) and all its samples had an arsenic level of less than 10μg/L. The groundwater in the Horinger platform zone was receiving platform recharge, with an arsenic concentration of 2.76μg/L. The groundwater in the Daqing Mountain piedmont alluvial plain zone had an arsenic concentration of 2.87μg/L. Samples collected in The transition zone had an arsenic concentration of 4.30μg/L. The groundwater in the Dahei River alluvial plain zone gathered in the discharge zone of the Dahei River alluvial plain, possessing the highest arsenic distribution in the Basin. The median value of its arsenic concentration was 54.3μg/L and the arsenic concentration of 79.5% of samples collected in this zone exceeded 10μg/L. The drainage canal zone was located near the Hasuhai Lake and the drainage canal, with an arsenic concentration of 2.48μg/L.

In the Dahei River alluvial plain, the groundwater runoff was slow and the lateral recharge was weak. Arsenic was released into the groundwater through the reductive dissolution of iron oxide in this strong reducing environment. At the same time, the strong evaporation and concentration due to the shallow water level would further lead to arsenic enrichment. High phosphate concentration also contributed to the release of arsenic by competing with arsenic for adsorption sites. In the piedmont-alluvial plain and platform front area, the groundwater was affected by strong lateral recharge and weak cation exchange. The weak reducing state is not favorable for the dissolution of iron oxide in groundwater. Moreover, the significant increase in water level depth led to weaker evaporation. The evaporation of groundwater near the Hasuhai Lake and the drainage canal was intensive, but the oxidation of groundwater was significantly enhanced by the recharge of surface water with high oxygen content, resulting in difficult enrichment of arsenic.

Declarations

Declarations

of interests

Ethics approval

Not applicable.

Competing interests

The authors declare that they have no competing interests.

Consent for publication

Not applicable.

Consent to participate

Not applicable.

Funding

This research was financially supported by National Natural Science Foundation of China (41972262) and Hebei Natural Science Foundation for Excellent Young Scholars (D2020504032).

Author's contributions

Yu Ren: Data analysis; writing original draft

Acknowledgements

Sincerely thanks are given to the journal editors and anonymous reviewers for their valuable comments and suggested revisions.

References

1. Armstrong MG (2004) An integrated hydrogeological/hydrogeochemical approach to characterising groundwater zonations within a quaternary coastal deltaic aquifer. The Burdekin River delta, North Queensland, Queensland University of Technology
2. Chengcheng L, Xubo G, Siqi L, Jochen B (2020) A review of the distribution, sources, genesis, and environmental concerns of salinity in groundwater. Environ Sci Pollut Res 27(33):41157–41174
3. Clemens R, Peter F and G., G.R (2005) Background and threshold: critical comparison of methods of determination. Sci Total Environ 346(1):1–16
4. Danrui S, Xiaohu W, Jun W, Min W, Haijiao Y, Chuanqi Z (2021) Comprehensive probabilistic health risk assessment for exposure to arsenic and cadmium in groundwater. Environ Manage 67(4):779–792
5. Dongguang W, Fucun Z, Eryong Z, Cheng W, Shuangbao H, Yan Z (2013) Arsenic, fluoride and iodine in groundwater of China. J Geochem Explor 135:1–21
6. Huaming G, Bo Z, Guangcai W, Zhaoli S (2010) Geochemical controls on arsenic and rare earth elements approximately along a groundwater flow path in the shallow aquifer of the Hetao Basin, Inner Mongolia. Chem Geol 270(1):117–125
7. Huaming G, Bo Z, Yuan L, Zsolt B, Xiaohui T, Stefan N, Doris S (2011) Hydrogeological and biogeochemical constrains of arsenic mobilization in shallow aquifers from the Hetao basin, Inner

Mongolia. Environ Pollut 159(4):876–883

8. Huaming G, Chen L, Hai L, Jun BWR, Yinzhu Z (2013) Pathways of coupled arsenic and iron cycling in high arsenic groundwater of the Hetao basin, Inner Mongolia, China: An iron isotope approach. Geochim Cosmochim Acta 112:130–145
9. Huaming G, Dongguang W, Zeyun L, Yongfeng J, Qi G (2014) A review of high arsenic groundwater in Mainland and Taiwan, China: Distribution, characteristics and geochemical processes. Appl Geochem 41(1):196–217
10. Huaming G, Suzhen Y, Xiaohui T, Yuan L, Zhaoli S (2008) Groundwater geochemistry and its implications for arsenic mobilization in shallow aquifers of the Hetao Basin, Inner Mongolia. Sci Total Environ 393(1):131–144
11. Kirk ND (2002) Worldwide occurrences of arsenic in ground water. Science 296(5576):21432145
12. Kumar MB and T., S.K (2002) Arsenic round the world: a review. Talanta 58(1):201–235
13. L., S.P. and G., K.D. A review of the source, behaviour and distribution of arsenic in natural waters.Applied Geochemistry17(5),517–568
14. L., S.P., M., Z., G., Z. and Z., L. Mobilisation of arsenic and other trace elements in fluviolacustrine aquifers of the Huhhot Basin, Inner Mongolia.Applied Geochemistry18(9),1453–1477
15. Marco R, John M, Letizia F, Elisa ASG, Tullia B (2017) Pollutant sources in an arsenic-affected multilayer aquifer in the Po Plain of Italy: Implications for drinking-water supply. Sci Total Environ 578:502–512
16. María D-O, Mariano S, Carlos D, Inés G and J., M.P.F (2007) Background arsenic concentrations in Southeastern Spanish soils. Sci Total Environ 378(1):5–12
17. Qi G, Huaming G, Yuance Y, Shuangbao H, Fucun Z (2014) Hydrogeochemical contrasts between low and high arsenic groundwater and its implications for arsenic mobilization in shallow aquifers of the northern Yinchuan Basin, P.R. China. J Hydrol 518:464–476
18. Scott F, Alexander vG (2010) Spatial and Temporal Variations of Groundwater Arsenic in South and Southeast Asia. Science 328(5982):1123–1127
19. Shuangbao H, Fucun Z, Hui Z, Yonghui A, Yushan W, Xi W, Cheng W (2013) Spatial and temporal patterns of groundwater arsenic in shallow and deep groundwater of Yinchuan Plain, China. J Geochem Explor 135:71–78
20. Silvera SAN, Rohan TE (2007) Trace elements and cancer risk: a review of the epidemiologic evidence. Cancer Causes Control 18:7–27
21. Søren J, Dieke P, Flemming L, Quy NP, Quynh HL, Kim TPT, Vu LT, Hung VP, Rasmus J (2012) Surface complexation modeling of groundwater arsenic mobility: Results of a forced gradient experiment in a Red River flood plain aquifer, Vietnam. Geochim Cosmochim Acta 98:186–201
22. T., R., P., B., C., M. and L., K. Assessment of the importance of dissimilatory nitrate reduction to ammonium for the terrestrial nitrogen cycle.Biogeosciences8(7),1779–1791

23. Ting L, Shan H, Jinli C, Haixia T, Chuanyong J (2012) Comparison of arsenic geochemical evolution in the Datong Basin (Shanxi) and Hetao Basin (Inner Mongolia), China. Appl Geochem 27(12):2315–2323
24. Wengeng C, Huaming G, Yilong Z, Rong M, Yasong L, Qiuyao D, Yuanjie L, Ruike Z (2017) Controls of paleochannels on groundwater arsenic distribution in shallow aquifers of alluvial plain in the Hetao Basin, China. Sci Total Environ 613–614(1):958–968
25. Xianjun X, Andre E, Yanxin W, Zuoming X, Mengyu D, Chunli S (2009) Geochemistry of redox-sensitive elements and sulfur isotopes in the high arsenic groundwater system of Datong Basin, China. Sci Total Environ 407(12):3823–3835
26. Xiaodong H, Peiyue L, Yujie J, Yuanhang W, Zhenmin S, Vetrimurugan E (2020) Groundwater arsenic and fluoride and associated arsenicosis and fluorosis in China: occurrence, distribution and management. Exposure and Health 12(3):355–368
27. Yan Z, Martin S, Alexander vG, Ittai G, Kumar DR, James SH, Peter S, Uddin AKM (2004) Redox control of arsenic mobilization in Bangladesh groundwater. Appl Geochem 19(2):201–214
28. Yanxin W, Junxia L, Teng M, Xianjun X, Yamin D, Yiqun G (2020) Genesis of geogenic contaminated groundwater:As, F and I. Critical Reviews in Environmental Science and Technology
29. Yanxin W, Kunfu P, Scott F, Yamin D, Xianjun X (2019) Sedimentogenesis and hydrobiogeochemistry of high arsenic Late Pleistocene-Holocene aquifer systems. Earth Sci Rev 189:79–98
30. Yanxin W, Xianjun X, Andre MJTCLC, Xiangli E, Mengyu W, Junxia L (2014) Coupled iron, sulfur and carbon isotope evidences for arsenic enrichment in groundwater. J Hydrol 519:414–422
31. Yao L, Chen Y, Bo Z, Dou C, Haolin Y, Christiane N, Wen S, Yvonne O, Harald N, Huaming G (2022) Spatial variation in dissolved phosphorus and interactions with arsenic in response to changing redox conditions in floodplain aquifers of the Hetao Basin, Inner Mongolia. Water Res 209:117930
32. Yinzhu Z, Huaming G, Zhuo Z, Hai L, Yongfeng J, Yongsheng C (2018) Characteristics and implication of stable carbon isotope in high arsenic groundwater systems in the northwest Hetao Basin, Inner Mongolia, China. J Asian Earth Sci 163:70–79
33. Yongfeng J, Huaming G, Beidou X, Yonghai J, Zhuo Z, Rongxiao Y, Weixiong Y, Xiaolei X (2017) Sources of groundwater salinity and potential impact on arsenic mobility in the western Hetao Basin, Inner Mongolia. Sci Total Environ 601–602:691–702
34. Yongfeng J, Huaming G, Yuxiao J, Yang W, Yinzhu Z (2014) Hydrogeochemical zonation and its implication for arsenic mobilization in deep groundwaters near alluvial fans in the Hetao Basin, Inner Mongolia. J Hydrol 518:410–420
35. Yu C, Habibu A (2004) Cancer burden from arsenic in drinking water in Bangladesh. Am J Public Health 94(5):741–744
36. Zhipeng G, Haicheng W, Huaming G (2021) Unraveling influences of nitrogen cycling on arsenic enrichment in groundwater from the Hetao Basin using geochemical and multi-isotopic approaches. J Hydrol 595:125981

37. Shuangbao H, Fucheng L, Sai W, Haixue L, Lei Y, Jingtao L, Haoyong S, Xueqing Z, Changqing L, Xi W, Tao M, Shibo W, Minmin Z (2021) Groundwater resource and eco-environmental problem of the Yellow River Basin. Geol China 48(4):1001–1019
38. Xiaobo L, Shaogang D, Baiwei L, Haibo F, Zhengkui L, Liwei L (2017) Hydrogeoehemical characteristics and genesis of groundwater in the Tumochuan Plain of Inner Mongolia. Acta Geoscientica Sinica 38(6):919–929
39. Yu R, Wengeng C, Deng P, Shuai W, Zeyan L, Jincheng L (2021) Evolution characteristics and change mechanism of arsenic and fluorine in shallow groundwater from a typical irrigation area in the lower reaches of the Yellow River (Henan) in 2010–2020. Rock and Mineral Analysis 40(6):846–859

Tables

Table 1
Distribution of main ion concentrations in groundwater

	Maximum	Minimum	Mean	Median
K^+(mg/L)	43.9	0.620	4.45	2.59
Ca^{2+}(mg/L)	260	5.70	56.0	49.1
Na^+(mg/L)	2.10×10^3	9.93	254	98.3
Mg^2(mg/L)	417	2.70	63.2	35.3
HCO_3^-(mg/L)	2.12×10^3	117	539	378
SO_4^{2-}(mg/L)	1.55×10^3	1.99	163	63.0
Cl^-(mg/L)	2.06×10^3	7.79	204	47.8
NO_3^-(mg/L)	537	0.100	45.7	6.82
TDS(mg/L)	6.11×10^3	262	1.09×10^3	579
pH	9.05	7.25	7.81	7.73
As(μg/L)	357	5.00×10^{-2}	26.9	3.15

Table 2
The meaning of different ion ratios and the distribution of arsenic

Ion ratio	Distribution range	Implication	Median arsenic concentration(μg/L)	The proportion of high arsenic(%)
$(HCO_3^- + CO_3^{2-})/SO_4^{2-}$	< 2	The environment of weak reduction	2.48	19.0
	2–10	The environment of medium reduction	3.36	19.7
	> 10	The environment of strong reduction	54.3	79.5
$Ca^{2+}/(HCO_3^- + CO_3^{2-})$	< 0.1	Weak lateral/surface water recharge intensity	54.3	79.5
	0.1–0.7	Medium lateral/surface water recharge intensity	3.36	19.7
	> 0.7	Strong lateral/surface water recharge intensity	0.785	0
Na^+/Ca^{2+}	< 1.1	Weak cation exchange	2.48	19.0
	> 13	Strong cation exchange	54.3	79.5
Ca^{2+}/Mg^{2+}	0.4–1.4	Medium lateral recharge intensity	3.38	14.0
	> 1.4	Strong lateral recharge intensity	0.785	0

Figures

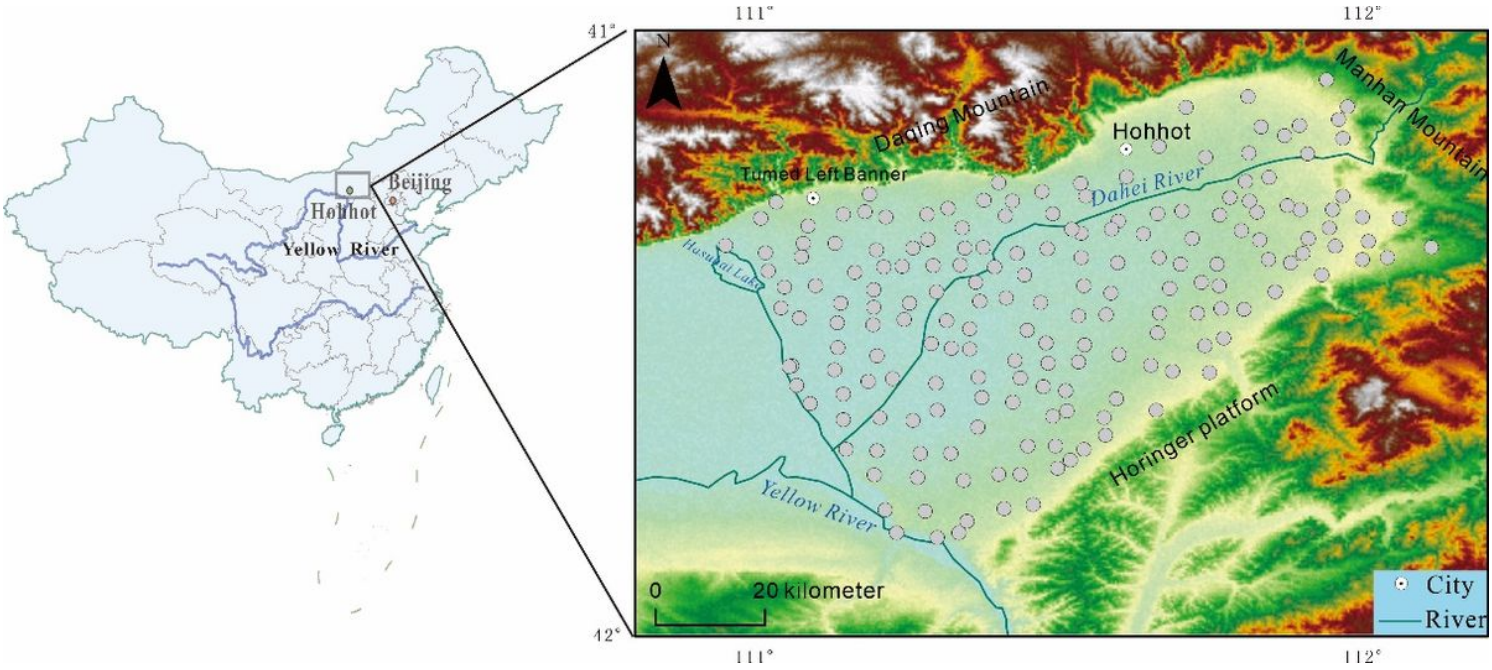

Figure 1

Geographical location of the Hohhot Basin

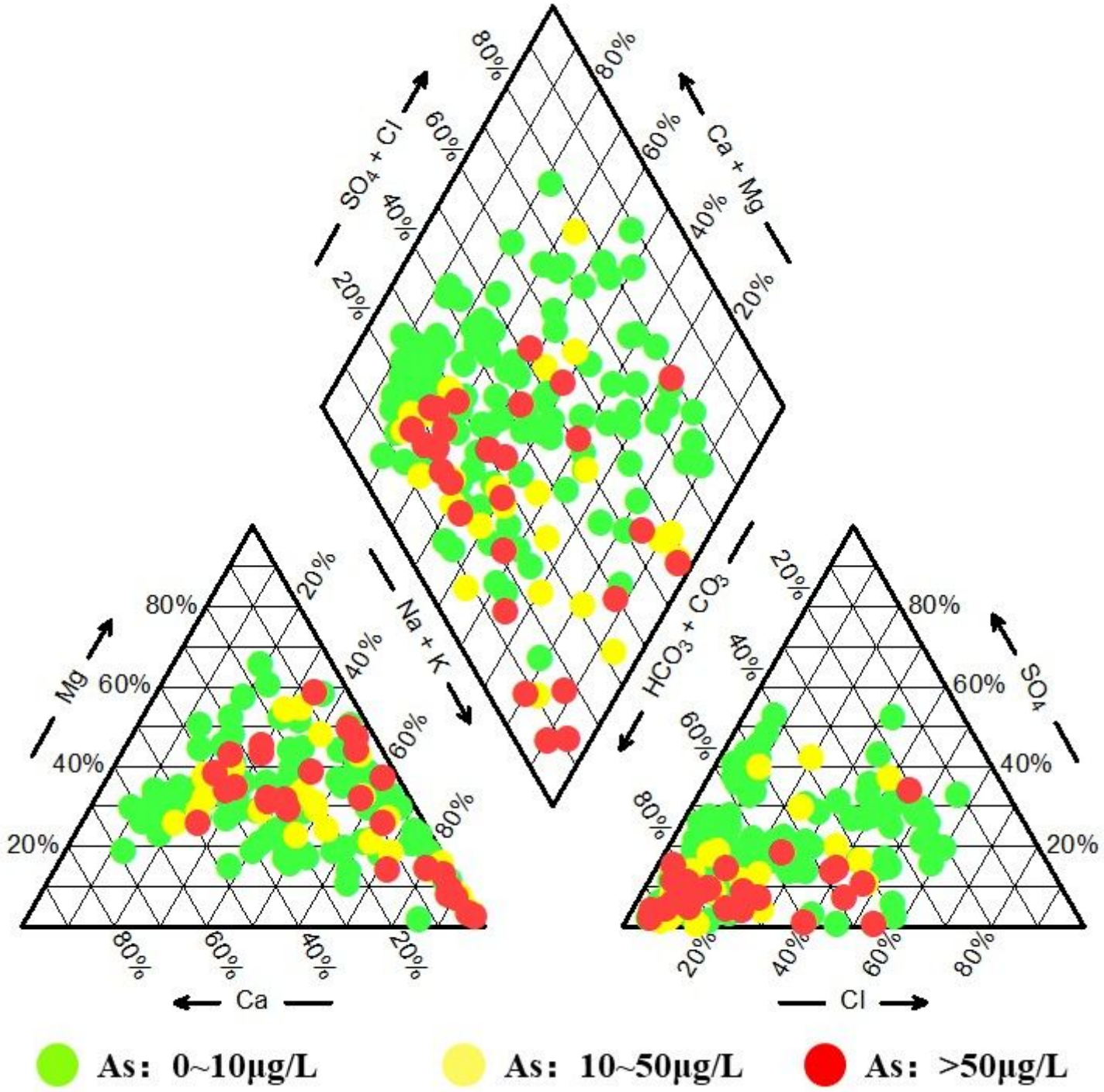

Figure 2

Piper diagram of shallow groundwater in the study area

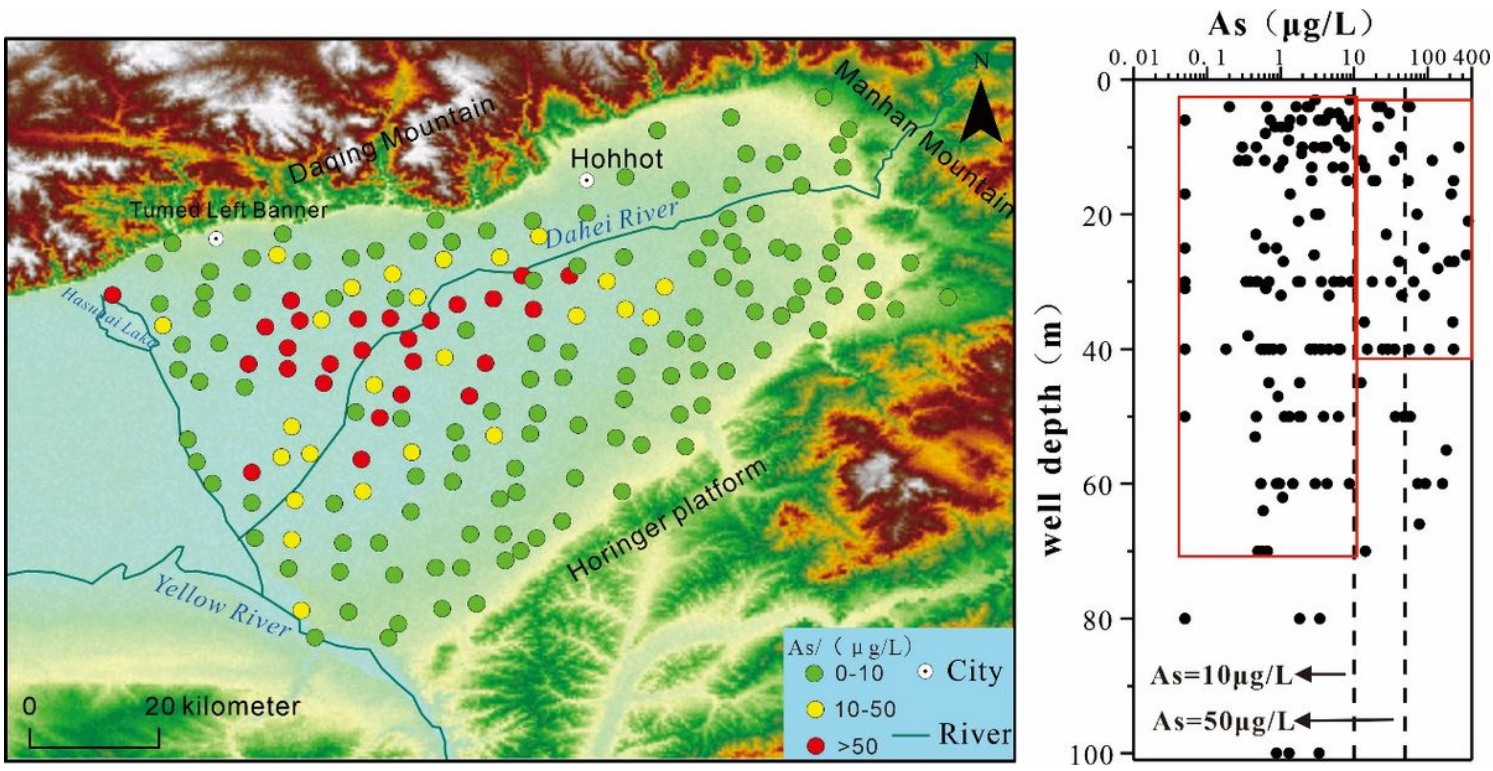

Figure 3

Spatial distribution of arsenic in groundwater and its relationship with well depth

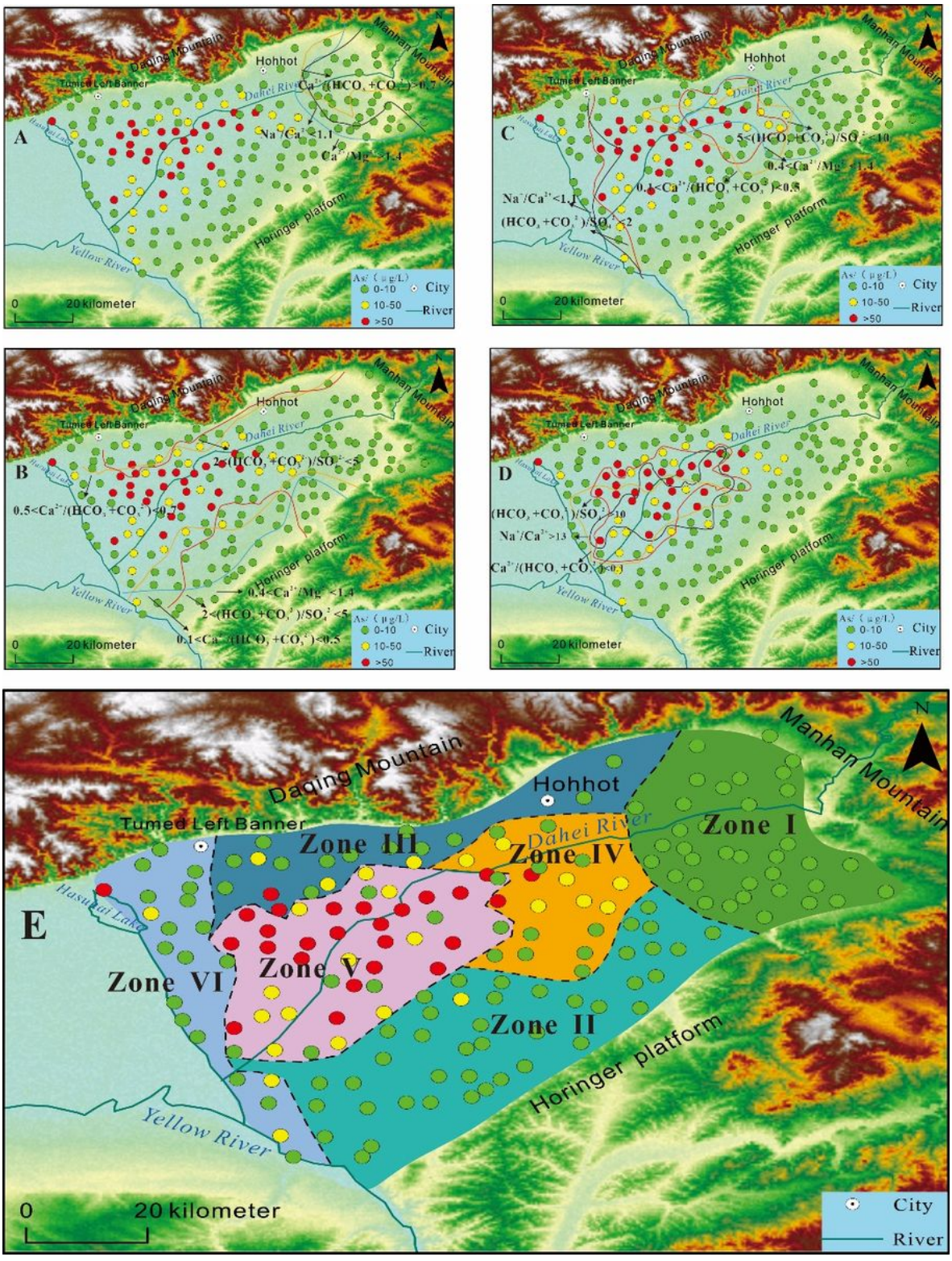

Figure 4

Cumulative frequency curve of $(HCO_3^- + CO_3^{2-})/SO_4^{2-}$, distribution of ratio groups and hydrochemistry types

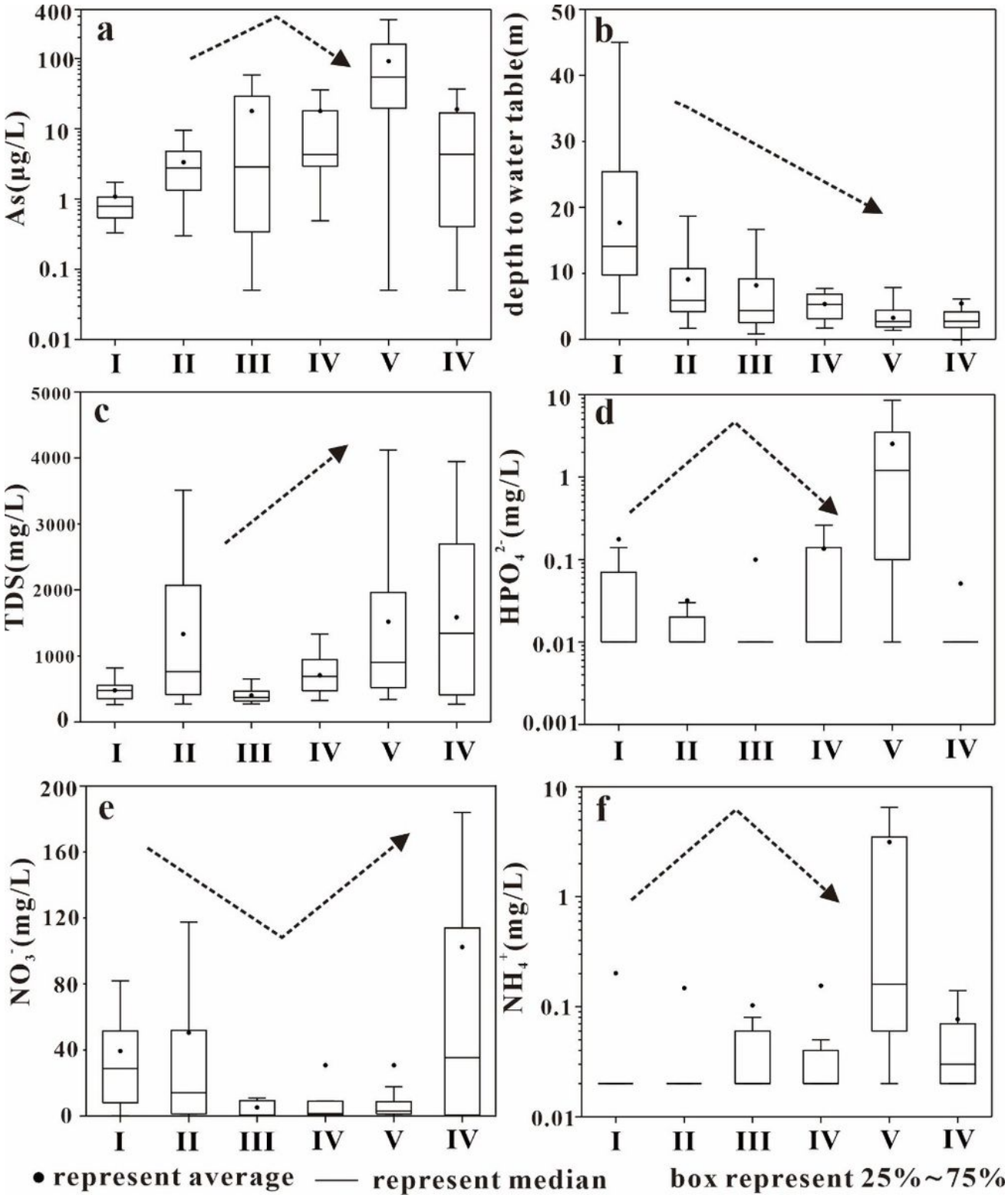

Figure 5

Cumulative frequency curve of $Ca^{2+}/(HCO_3^-+CO_3^{2-})$, distribution of ratio groups and hydrochemistry types

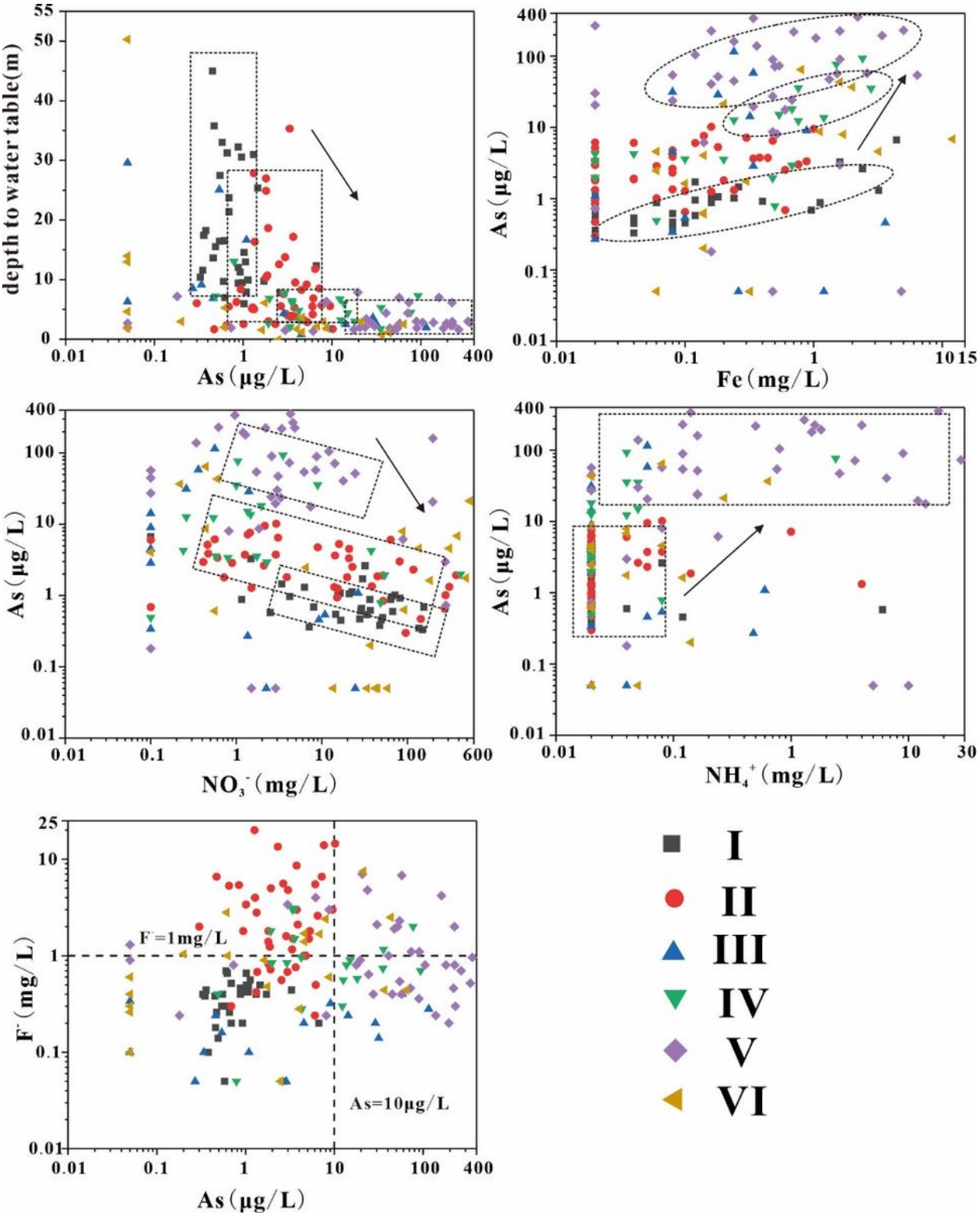

Figure 6

Cumulative frequency curve of Ca^{2+}/Mg^{2+}, distribution of ratio groups and hydrochemistry types

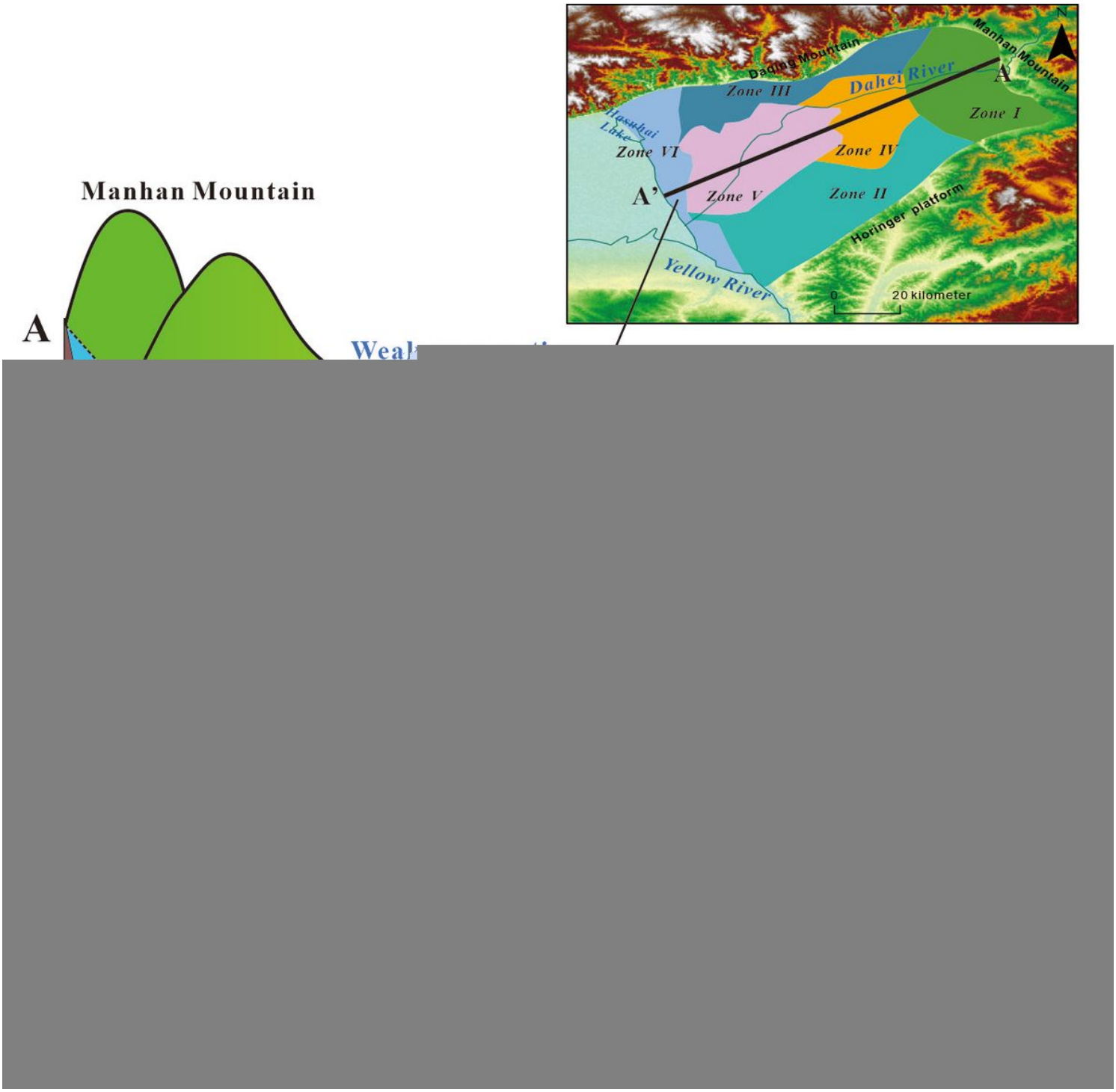

Figure 7

Cumulative frequency curve of Na^{+}/Ca^{2+}, distribution of ratio groups and hydrochemistry types

Figure 8

Ion ratio distribution and regional recognition in shallow groundwater

Supplementary Files

This is a list of supplementary files associated with this preprint. Click to download.

- SupplementaryMaterial.docx